Morphological Control of Freeze-Structured Scaffolds by Selective Temperature and Material Control in the Ice-Templating Process

Annika Seifert, Julia Gruber, Uwe Gbureck,* and Jürgen Groll*

Herein, it is aimed to highlight the importance of the process parameter choice during directional solidification of polymer solutions, as they have a significant influence on the pore structure and orientation. Biopolymer solutions (alginate and chitosan) are directionally frozen, while systematically varying parameters such as the external temperature gradient, the temperature of the overall system, and the temperatures of the cooling surfaces. In addition, the effect of material properties such as molecular weight, solution concentration, or viscosity on the sample morphology is investigated. By selecting appropriate temperature gradients and cooling surface temperatures, aligned pores ranging in size between (50 ± 22) µm and (144 ± 56) µm are observed in the alginate samples, whereas the pore orientation is influenced by altering the external temperature gradient. As this gradient increases, the pores are increasingly oriented perpendicular to the sample surface. This is also observed in the chitosan samples. However, if the overall system is too cold, that is, using temperatures of the lower cooling surface down to $-60\,^{\circ}\text{C}$ combined with low temperatures of the upper cooling surface, control over pore orientation is lost. This is also found when viscosity of chitosan solutions is above ≈ 5 Pas near the freezing point.

1. Introduction

Ice templating, also often referred to as freeze casting or freeze-structuring, is a very straightforward, simple, low-cost, and versatile process for the fabrication of highly porous scaffolds with an anisotropic pore structure. Due to the wide range of

A. Seifert, J. Gruber, U. Gbureck, J. Groll
Department for Functional Materials in Medicine and Dentistry at the
Institute of Functional Materials and Biofabrication
University of Würzburg
Pleicherwall 2, Würzburg D-97070, Germany
E-mail: juergen.groll@fmz.uni-wuerzburg.de

U. Gbureck
Zentrum für Zahn-, Mund- und Kiefergesundheit Lehrstuhl für
Funktionswerkstoffe der Medizin und der Zahnheilkunde
Universitätsklinikum Würzburg
Pleicherwall 2, Würzburg 97070, Germany
E-mail: uwe.gbureck@fmz.uni-wuerzburg.de

The ORCID identification number(s) for the author(s) of this article can be found under https://doi.org/10.1002/adem.202100860.

applications of scaffolds produced by ice templating, a large number of research articles and reviews exist,[1–10] highlighting the increasing importance of this emerging process in recent years. Scaffolds with aligned porosity are highly interesting for various fields, from supercapacitors,[11–14] electrodes in batteries,[15,16] or thermal insulators[17,18] to biomaterials for tissue engineering,[19–22] 3D cell culture,[23] or as cell-containing solid-state scaffolds.[24]

There are different ways of ice templating.[7] In the conventional unidirectional freezing method, a single temperature gradient is superimposed on the sample during freezing, whereby ice crystallization begins in a disordered manner on the cooled surface, resulting in a scaffold with an anisotropic structure in vertical direction and with several domains of different orientations in the horizontal plane.[25,26] A further possibility is bidirectional freezing,[26,27] where dual temperature gradients cause the ice to propagate both horizontally and vertically, resulting in a large-scale uniform scaffold structure. In addition, there are other approaches to influence the horizontal domain orientation,[7] such as radial,[28] magnetic,[29] electrical,[30] or ultrasonic freeze casting,[31] all of which lead to various morphologies of the resulting scaffolds and require different complex technical equipment.[7] This demonstrates the wide range of possibilities for the resulting scaffold morphology through the choice of an appropriate freezing process.

A major advantage of unidirectional freezing is that this easy-to-use process does not require complex and costly laboratory equipment. In general, a solution, suspension, or slurry is frozen in the presence of an external temperature gradient. Solutes are forced between the growing ice lamellae. After removal of the ice crystals by freeze drying, the scaffold represents a negative of the original ice morphology.[32] Consequently, a highly anisotropic porous sample is obtained. The morphological properties, such as vertical pore orientation or pore size of the scaffolds, play a decisive role depending on the application in which the scaffold is intended to be used. In terms of pore size, pores can be generated at different size scales, with pore diameters well above 100 µm being feasible.[33,34]

Scaffolds, which are to be used as bone substitute materials in tissue engineering applications, may serve as an example. Values of at least 100 µm up to several hundred micrometers (> 300 µm) are considered optimal pore sizes for cell ingrowth, nutrient and

oxygen supply, and subsequent vascularization.[35–37] All these parameters are positively affected by the use of ice-templated scaffolds with a highly ordered anisotropic pore structure[38,39] and can therefore be adjusted by choosing the right pore properties.

In addition, orientation of the pores is of significance. Thus, by varying the temperature gradients and hence the pore orientation, a monolithic anatomically shaped meniscus was fabricated using unidirectional freeze-structuring.[34]

Whether specifically for the use as biomaterials or for any of the other various applications mentioned earlier, a fundamental knowledge of the relationship between freezing parameters and pore size and orientation is important for unidirectional freeze-structuring. Thereby, it is important to note that the choice of material and material properties has a direct influence on the resulting pores. In this study, a custom-built device (patented process[34,40]) was used to ice template alginate or chitosan solutions in the presence of an external temperature gradient, which was varied systematically. Several material parameters such as polymer concentration in the solution, molecular weight (MW), and hence viscosity were altered. The resulting pore morphology was assessed as a function of the polymer properties as well as different freezing parameters such as temperature gradient, cooling rate, and absolute temperatures of the cooling surfaces.

2. Experimental Section

2.1. Freeze-Structuring Device

The in-house developed freeze-structuring system that was used for the ice-templating process in this study (**Figure 1**a–c) basically consisted of a copper block and a copper lid, which can be opened and closed pneumatically for injecting the solutions. The core of the freeze-structuring unit included two superimposed Peltier elements (PEs). These were connected to two laboratory power supplies ("PSP 12 010," Voltcraft, Wollerau, Switzerland), which provided the PEs with the current necessary for the selected temperatures.

3 mL of the polymer solution was poured into a sample container located between the PEs and directionally frozen. Both the PEs and the sample were surrounded by a polyether ether ketone (PEEK) thermal isolation unit, which allowed for the generation of a directional external temperature gradient. This gradient was created by varying the temperature of the PEs, with the lower PE always being colder than the upper PE for all experiments. Thus, the heat flow occurred in the direction from the upper to the lower PE, which also corresponded to the direction of the external temperature gradient described by Equation (1).[34]

$$\vec{\nabla} T = \frac{\partial T}{\partial \vec{x}} \cong \frac{|T_{\text{upper PE}} - T_{\text{lower PE}}|}{\vec{x}_{\text{upper PE}} - \vec{x}_{\text{lower PE}}} \tag{1}$$

Here, $T_{\text{upper PE}}$ is the temperature of the upper and $T_{\text{lower PE}}$ of the lower PE. $\vec{x}_{\text{upper PE}}$ and $\vec{x}_{\text{upper PE}}$ represent the corresponding position vectors of the PEs. As only the gradient perpendicular to the surfaces of the PEs was considered, the temperature gradient was expressed as a scalar in the following.[34] This external temperature gradient generated by the PEs was superimposed by the latent heat released during the freezing of the solution. Consequently, a distinction must be made between the external and the internal, resulting temperature gradient. However, the internal temperature gradient is not determined within the scope of this study. Therefore, the values given in the further course of this work describe the magnitude of the external temperature gradient.
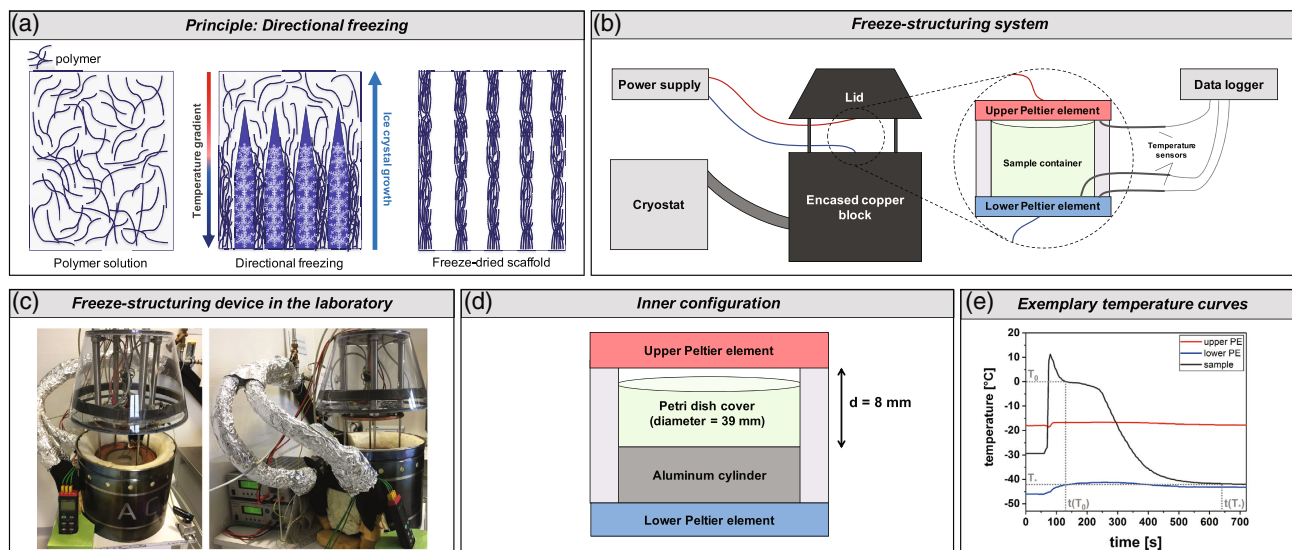

Figure 1. Directional freezing with a custom-built device. a) In directional freezing, a polymer solution is frozen in the presence of a temperature gradient. After freeze drying, a porous scaffold with anisotropic porosity is obtained. b) The in-house-developed freeze-structuring system consisted of a copper block coupled to a cryostat. The sample was located between two PEs that were tempered differently to generate an external temperature gradient. Three temperature sensors measured the PE and sample temperatures. c) Photograph of the freeze-structuring device in the laboratory. d) A Petri dish cover with a diameter of 39 mm served as a sample container and was placed on an aluminum cylinder. e) Exemplary measurement curves of PE and sample temperatures (upper PE [red], lower PE [blue], sample [black]) during directional freezing. The temperature of the completely frozen sample T_* as well as the temperature T_0 (0 °C) and the corresponding time points $t(T_*)$ and $t(T_0)$ are indicated in gray.

Table 1. PE temperature differences required for the different temperature gradients.

Temperature gradient [K mm^{-1}]	Temperature difference [K]
1	8
1.5	12
2	16
2.5	20
3	24
3.5	28
4	32

The lower PE was in thermal contact with the cylindrical copper block, which was coupled to a cryogenic environmental thermostat ("FPW 91," Julabo, Seelbach, Germany) and perfused by coolant ("Thermal HY," Julabo, Seelbach, Germany). The choice of the coolant temperature was also used to vary the temperature of the overall system and thus the limits of the temperatures that were achievable by the PEs. As the temperature of the lower PE reached a plateau at a certain threshold voltage, the temperature of the coolant flowing through the copper block determined the minimum temperature of the lower PE. This in turn was decisive for the choice of the temperature of the upper PE at a given temperature gradient (see Equation (1)).

The sample container used in this work was a petri dish cover with a diameter of 39 mm and a height of 5 mm. Figure 1d shows a schematic side view of the setup used for sample fabrication in this study. Due to a built-in heat-conducting aluminum cylinder on which the cover was placed, a PE distance of 8 mm was assumed for the calculation of the external temperature gradient. The temperature differences of the PEs required for the respective temperature gradients are shown in **Table 1**.

In this study, two different series of experiments were conducted for the directional freezing of alginate solutions. In experiments 1–4, the temperature of the upper PE remained largely constant for all temperature gradients, whereas the temperature of the lower PE changed, while this was the opposite for experiments 5–7. The experiments were conducted at different temperature regimes, where the temperatures were determined by the coolant temperature in the freeze-structuring unit. The coolant temperatures used for each experiment are shown in **Table 2**.

Table 2. Coolant temperatures used for the directional freezing of alginate solutions. The temperatures of the coolant determined the temperature of the overall system.

	Temperature of upper PE	Temperature of lower PE	Coolant temperature [°C]
Experiment 1	Identical	Variable	−47
Experiment 2	Identical	Variable	−33
Experiment 3	Identical	Variable	−30
Experiment 4	Identical	Variable	−25
Experiment 5	Variable	Identical	−47
Experiment 6	Variable	Identical	−40
Experiment 7	Variable	Identical	−33

Temperatures were measured with three sensors inside the freeze-structuring device. Two temperature sensors were in contact with the upper and lower PE, respectively, to measure the temperatures of the PEs and consequently the temperature gradient. A third temperature sensor was located in the sample and monitored the temperature profile during the freezing process. To ensure the same position of this sensor for each experiment, it was bent in such a way that the tip touched the bottom of the Petri dish. The sensors were connected to a datalogger ("K204 Datalogger," Voltcraft, Wollerau, Switzerland), which recorded the temperature curve over time (Figure 1b).

2.2. Temperature Curves and Cooling Rate

Exemplary measurement curves of the PE temperatures as well as the temperature within the sample measured by the temperature sensors are shown in Figure 1e. At the beginning of every experiment, the selected temperatures of the upper PE (red line) and the lower PE (blue line) were set. When the system was in thermal equilibrium, the polymer solution was injected and the temperature within the sample (black line) was measured. Using these temperature curves, the cooling rate v_c, which describes the heat removal per time unit from the sample, can be calculated from Equation (2).[34]

$$v_c = \frac{T_* - T_0}{t(T_*) - t(T_0)} \qquad (2)$$

According to Stuckensen et al., T_* corresponds to the temperature of the completely frozen sample, which is defined as the temperature in which the frozen sample is first kept constant for at least 30 s. The starting point of this level is given by the time $t(T_*)$. Accordingly, $t(T_0)$ corresponds to the time at which the sample reaches the temperature $T_0 = 0\,°C$.[34]

The temperature gradient was calculated according to Equation (1) and from the arithmetic mean of the PE temperatures at times $t(T_*)$ and $t(T_0)$.

For each setting and sample type, three samples were freeze structured. The mean values of the cooling rate and the temperature gradient were given with standard deviation.

2.3. Freeze Drying

After freezing, the samples were freeze dried at −57 °C and a maximum of 1 mbar ("Alpha 1–2 LDplus," Christ, Osterode am Harz, Germany).

2.4. Polymer Solutions

2.4.1. Preparation of Polymer Solutions

The alginate solutions had a concentration of 2% (w/w) and were prepared by dissolving sodium alginate powder ("Protanal LF 10/60FT," FMC Biopolymer, Philadelphia, USA) in ultrapure water.

The solvent for the chitosan powders was 1% (v/v) acetic acid prepared by diluting acetic acid (≥ 99.8%, Sigma-Aldrich, St. Louis, USA) in ultrapure water. A total of three different chitosan solutions was prepared. Solutions containing low-MW chitosan (Sigma-Aldrich, St. Louis, USA) were obtained by dissolving the chitosan powder at both 2% (w/w) and 4% (w/w) concentrations

Table 3. MWs and dispersity of alginate used for the systematic investigations.

	MW [kDa]			Dispersity
	M_n	M_w	M_z	
Alginate Protanal LF 10/60 FT	99.9	156.9	248.6	1.572

in 1% (v/v) acetic acid. In addition, a 2% (w/w) chitosan solution was prepared from high-MW chitosan powder (Sigma-Aldrich, St. Louis, USA).

After complete dissolution of the powders, solutions were centrifuged ("Mega Star 1.6 R," VWR, Radnor, USA) for 5 min at room temperature and 4500 rpm to remove any air bubbles present in the solution.

2.4.2. MW and Dispersity

The MW and dispersity of the alginate were determined using an aqueous gel permeation chromatography (GPC) system (Malvern, Herrenberg, Germany) and are shown in **Table 3**. Here, M_n is the number average, M_w the weight average, and M_z the centrifuge average.

Alginate powder was dissolved at a concentration of $1\,\mathrm{mg\,L^{-1}}$ in an aqueous solution of $8.5 \times \mathrm{g\,L^{-1}}$ NaNO$_3$ and $0.2 \times \mathrm{g\,L^{-1}}$ NaN$_3$, which was also used as eluent, for 24 h. Prior to measurement, solutions were filtered through a 0.45 µL cellulose filter. Subsequently, 100 µL of the respective solutions was measured using a GPC system containing the following components: Viscotek GPCmax, column oven (35 °C), "Viscotek VE3580" refractive index detector, "Viscotek SEC-MALS 20," two "A6000M" Viscotek A-columns (length = 300 mm, width = 8 mm, porous polymethyl methacrylate, particle size: 13 µm). After calibration with polyethylene glycol standards, data were evaluated with the MALS calibration.

The MW of the low-MW chitosan was reported by the manufacturer to be 50–190 kDa, whereas that of the high MW chitosan was specified as 310–375 kDa.

2.4.3. Determination of Viscosity as a Function of Temperature

The temperature-dependent viscosity of the polymer solutions used for freeze-structuring was determined using a rheometer ("MCR702," Anton Paar, Graz, Austria) at a parallel plate geometry with a diameter of 25 mm and a plate distance of 0.5 mm. Solutions were cooled from 25 °C to 0 °C at a cooling rate of $4\,\mathrm{K\,min^{-1}}$ during the measurement. Three measurements were taken for each solution type and the arithmetic mean value of viscosity was plotted with the standard deviation as a function of temperature.

2.5. Sample Characterization

2.5.1. Imaging

Prior to imaging of the sample surface or cross section, scaffolds were cut using a razor blade. Sample sections were first examined using the "SteREO Discovery.V20" stereomicroscope (Zeiss, Jena, Germany) and the associated "ZEN2012 pro" software. Samples were then fixed with the cement "Leit C Conductive Carbon Cement" (PLANO GmbH, Wetzlar, Germany) on scanning electron microscopy (SEM) specimen holders (Agar Scientific, Stansted, UK). A high vacuum coater ("EM ACE600," Leica, Wetzlar, Germany) was used to apply a 6 nm thick platinum layer with a current of 35 mA to avoid electrical charging of the samples during imaging using a scanning electron microscope ("Crossbeam 340" Zeiss, Jena, Germany).

2.5.2. Pore Size Determination

The pore diameters were measured manually using the software "ImageJ." For this purpose, a representative SEM image of the cross section was taken at 50× magnification for each sample. The broadest area of each individual pore visible on the image was then measured. The arithmetic mean of the measured values with standard deviation was defined as the pore diameter.

3. Results

3.1. Alginate

3.1.1. a-Factor and Cooling Rate

One objective of the systematic investigations in this study was to reveal the influence of the absolute PE temperatures used for the respective temperature gradients on the cooling rates as well as on the resulting sample morphology of alginate samples.

The cooling rate during freezing is an important parameter in directional freezing, as it affects the resulting pore size and scaffold morphology.[41,42] However, the magnitude of the external temperature gradient, which influences pore orientation, also plays an important role. As a temperature gradient is defined only by the temperature difference and the distance of the PEs, there is a multitude of possible PE temperatures to be able to set the same temperature gradient. Here, it is only of crucial importance that the temperature difference calculated based on Equation (1) is maintained. Therefore, alginate solutions with a concentration of 2% (w/w) were used to systematically investigate how the choice of PE temperatures affects the course of the cooling rate as a function of the external temperature gradient.

For this, two different series of experiments were conducted. In series of experiments 1, the temperature of the upper PE remained almost the same for all temperature gradients, whereas the temperature of the lower PE gradually decreased for larger temperature gradients. Deviations at low temperature gradients were due to technical reasons. The experiments were conducted for different temperature ranges. The overall system was coldest for experiment 1 and warmest for experiment 4. (**Figure 2**a and Table 2)

Temperatures in series of experiments 2 were chosen inversely. The temperature of the lower PE remained the same for all temperature gradients, whereas that of the upper PE gradually increased for higher temperature gradients. (Figure 2d) Different temperature ranges were also selected in these experiment series. The overall system was coldest in experiment 5 and warmest in experiment 7.
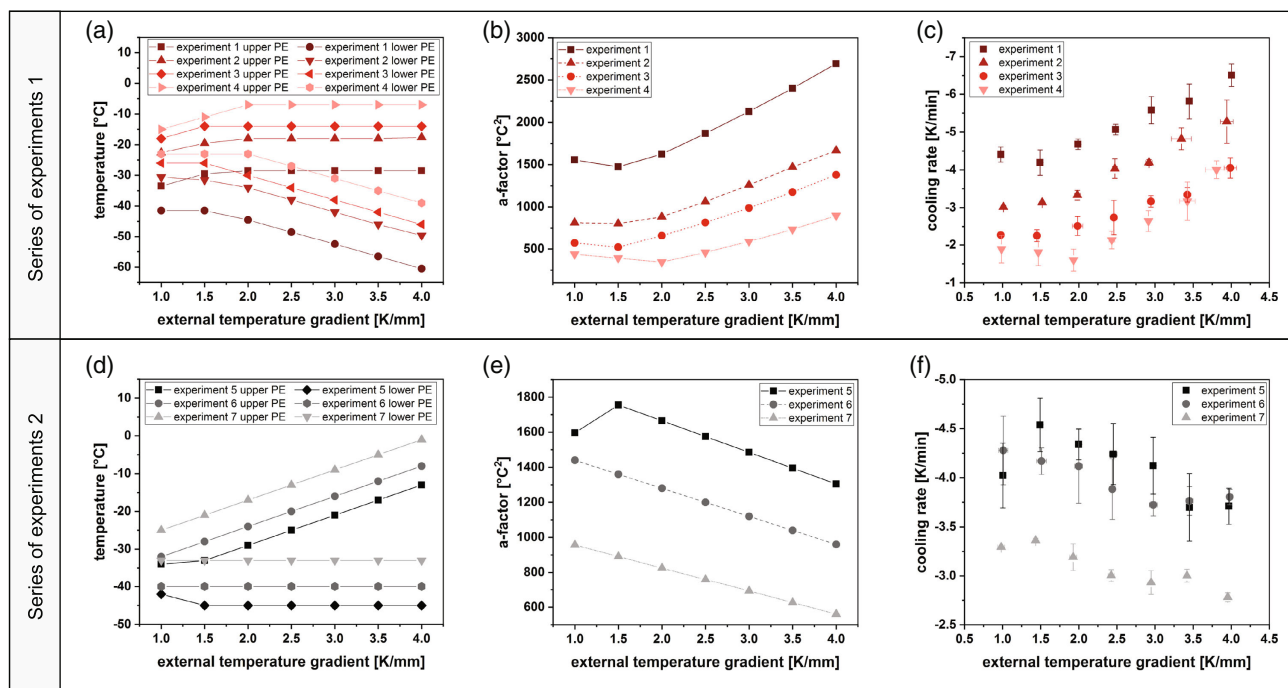
Figure 2. Cooling rate and a-factor of directionally frozen alginate samples. a) The temperatures of the upper PE were largely the same for the series of experiments 1, whereas the temperatures of the lower PE were gradually lowered for higher temperature gradients. b) The calculated course of the a-factor as a function of the external temperature gradient was confirmed by the c) experimental determination of the cooling rates. d) In series of experiments 2, the temperature of the lower PE was nearly constant for all temperature gradients, whereas that of the upper PE was gradually increased for higher gradients. e) The cooling rates theoretically predicted by the a-factor decreased with increasing temperature gradient, f) which was also observed experimentally.

In this study, a factor that includes the average temperature of the PEs, and is therefore referred to as the average (a-)factor, was developed (Equation (3)). By including the PE average temperature, the total temperature of the system is considered. In addition, the absolute temperature of the lower cooling surface, which is in direct contact with the sample, is taken into account. The freezing process and consequently the nucleation of ice crystals start at the lower surface. With the help of this a-factor, it is possible to predict the course of cooling rates as a function of the external temperature gradient at given PE temperatures.

$$a = \frac{T_{\text{upper PE}} + T_{\text{lower PE}}}{2} \cdot T_{\text{lower PE}} \quad (3)$$

The development of this a-factor offers the advantage that, for given parameters, the magnitude and course of the cooling rates, and thus to some extent the morphology of the samples, such as pore orientation and size, can be predicted. Figure 2b and e show the a-factor as a function of the temperature gradient. For experiment series 1, it became clear that the a-factor increased with increasing temperature gradient and was generally higher for colder overall systems. The curve for experiment 1 was the highest, whereas the courses of the experiments with warmer overall systems were below it in the corresponding order. (Figure 2b) For the series of experiment 2, the a-factor decreased with increasing temperature gradients. Again, the temperature range

of the system had an effect on the magnitude of the a-factor. (Figure 2e)

The courses of the cooling rates predicted by the a-factor could be confirmed experimentally for both experimental series. (Figure 2c,f) The colder the overall system, the higher the cooling rates observed.

3.1.2. SEM and Pore Size Distribution

The impact of the various freezing parameters such as temperature gradients, cooling rates, and overall system temperatures and their effect on pore orientation and size is of significant interest.

SEM imaging of the samples was used to assess the pore orientation and size. In the following, the term "pore size" always refers to the pore diameter measured in the SEM cross-section images of the samples. The lamellar pore structure that is characteristic for the directionally frozen samples was revealed by combining SEM imaging of the surfaces of four exemplary samples from experiment 2 (**Figure 3**) with imaging of sample cross sections. (**Figure 4**) Highly porous samples with anisotropic continuous pores were observed independently of the temperature gradient and the PE temperatures during the freezing process.

Figure 4a shows the samples associated with experiments 1–4, in which the upper PE had nearly the same temperature for all temperature gradients, whereas the temperature of the lower PE was gradually lowered for higher gradients. For experiment 1,
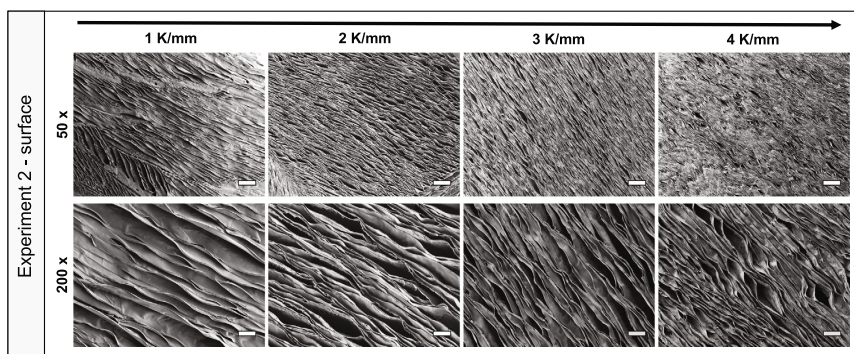
Figure 3. SEM surface images of alginate samples. Images of an exemplary sample series from experiment 2 show a lamellar pore structure. The top row shows one sample surface per temperature gradient at 50× magnification, whereas the sample surfaces at 200× magnification are presented in the bottom row. Scale bars are 200 μm in the top row and 50 μm in the bottom row.

where the overall system was the coldest and the highest cooling rates appeared, no distinct dependence of the pore orientation on the external temperature gradient was found. Examination of the corresponding images suggested that the structuring process was kinetically controlled using too low temperatures and that, in some cases, several domains of different orientations were formed in close proximity to each other. This was also found when examining larger sample sections using stereomicroscopy. (Figure 6a) However, for experiments 2–4, it became evident in both the SEM and stereomicroscope images (Figure 4a and Figure 6a) that the freezing process was well controlled. Pores were increasingly oriented perpendicular to the surface with increasing external temperature gradient (Figure 3, Figure 4a) and exhibited a uniform morphology.

The measurement of the pore sizes revealed for experiments 1–4 that the pore size was to a certain degree adjustable by the choice of suitable parameters. (Figure 4c) In general, a higher temperature gradient and higher cooling rates resulted in smaller pore sizes (Figure 4c, **Figure 5**a–d). Compared with experiment 1 with the highest cooling rates (Figure 5a), pore diameters were shifted toward higher values when lower cooling rates were used (experiment 4, Figure 5d). In this way, pore sizes between (50 ± 22) μm (temperature gradient: 4 K mm^{-1}, experiment 1) and (144 ± 56) μm (temperature gradient: 1 K mm^{-1}, experiment 4) could be obtained only by varying the freezing parameters. If the pore orientation is also taken into account, that is, only one gradient is considered, pore size differences of about 40 μm could be obtained in the various experiments.

Figure 4b shows the SEM images of the samples from experiments 5 to 7. Again, the tendency for the pores to be increasingly oriented perpendicular to the surface with increasing temperature gradient became evident. This was also visible in stereomicroscopic observation of larger sample sections, where nearly all scaffolds showed a uniform structuring. (**Figure 6**b) Consideration of the different temperature regimes showed that lower cooling rates tended to cause larger pores than higher cooling rates (Figure 4d, Figure 5e–g).

Comparing the two series of experiments, it can be concluded that the pore orientation does not depend on the temperatures of the PEs, but on the magnitude of the temperature gradient. The PE temperatures determine the resulting cooling rates, which in turn are responsible for the pore size. However, if the overall system is too cold (see experiment 1), control over the pore orientation is lost.

3.2. Chitosan

3.2.1. Viscosities

In addition to the systematic investigations with alginate solutions, experiments with a further biopolymer, chitosan, were conducted. Here, the focus was on the influence of various properties of the solution, such as concentration, MW of the polymer, and, as a result, viscosity, on the freeze-structuring process. For this purpose, two chitosan solutions of different concentrations (2% [w/w] and 4% [w/w]) of a low-MW chitosan were compared. Furthermore, the influence of MW on freeze-structuring was investigated using a 2% (w/w) solution of a high-MW chitosan. The effect of concentration and MW on viscosity during cooling of the solutions from room temperature to 0 °C is shown in **Figure 7**.

The 4% (w/w) solution of the low-MW chitosan had the highest viscosity of the solutions comparable. Depending on the temperature, this was between (7.11 ± 0.07) Pas at 25 °C and (14.91 ± 0.08) Pas near 0 °C. Lower values of (3.39 ± 0.06) Pas at 25 °C to (5.61 ± 0.04) Pas close to the freezing point were measured for the still highly viscous 2% (w/w) solution of the high-MW chitosan. In contrast, the 2% (w/w) solution of the low-MW chitosan was considerably less viscous with a viscosity from (0.490 ± 0.003) Pas to (1.401 ± 0.003) Pas, depending on the temperature.

For comparison, the viscosity of the alginate solution used for the systematic investigations described previously is shown in black. From (0.142 ± 0.001) Pas to (0.348 ± 0.002) Pas, it is clearly below the viscosities found for the chitosan solutions.

3.2.2. α-Factor and Cooling Rate

According to the freeze-structuring of alginate solutions, both process parameters, external temperature gradient and PE temperatures, were varied.

Two different temperature ranges were selected. In the case of PE temperatures 1 (**Figure 8**a), the temperature of the upper PE
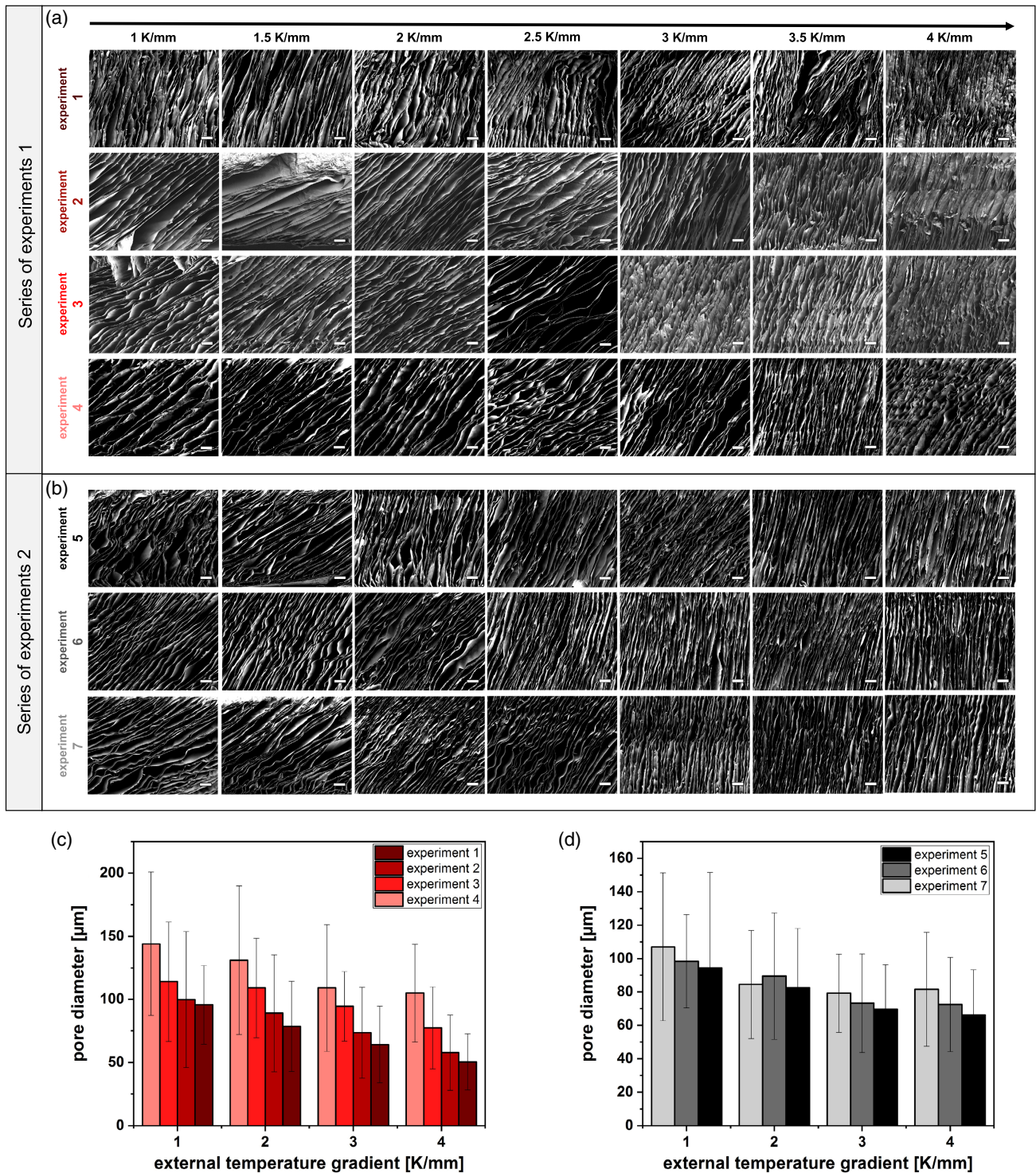
Figure 4. Pore orientation and diameter of directionally frozen alginate samples. a) SEM cross-section images of samples from experiment series 1. No clear dependence of the pore orientation on the external temperature gradient was observed for the samples of experiment 1. In experiments 2–4, the pores were increasingly oriented perpendicular to the surface as the temperature gradient increased. b) This trend was also observed for the samples of experiment series 2. c) The pore diameter of the samples from experiment series 1 decreased with increasing temperature gradient. Smaller pores were observed for colder systems. d) Similar was found for the samples of experiment series 2. Scale bars in (a) and (b) are 200 μm.
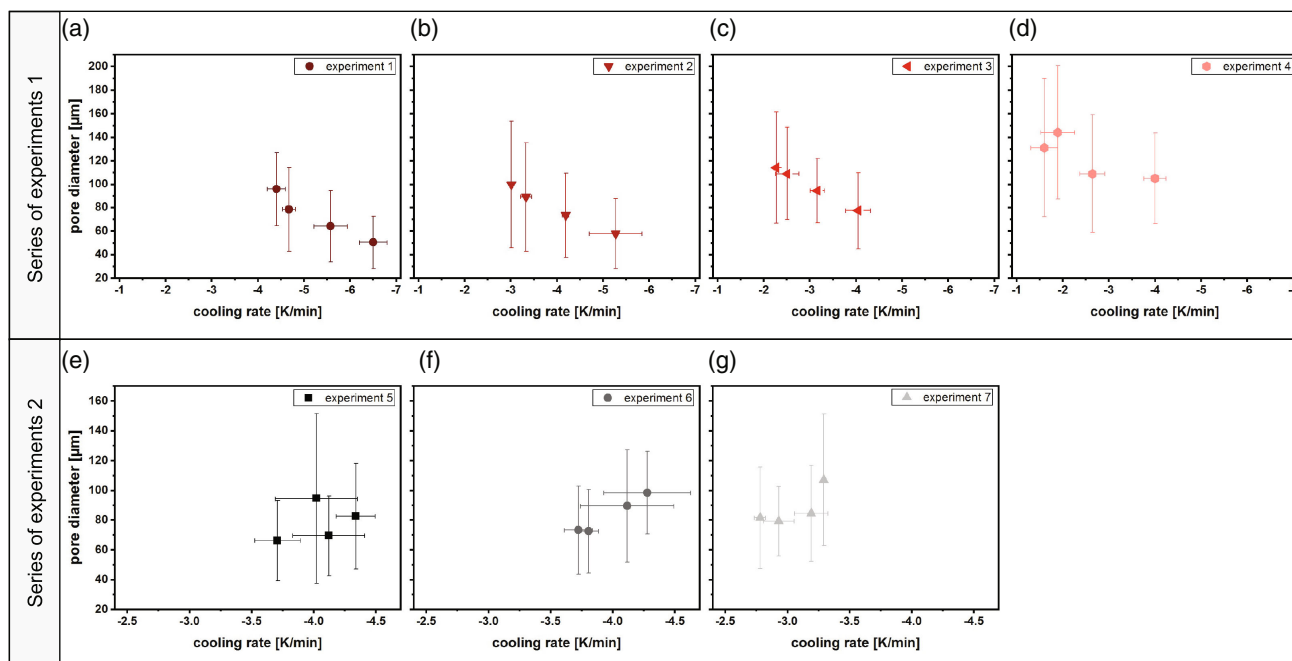
**ADVANCED
SCIENCE NEWS**

www.advancedsciencenews.com

**ADVANCED
ENGINEERING
MATERIALS**

www.aem-journal.com

Figure 5. Pore diameter of alginate samples as a function of cooling rate. For experiment series 1, the pore diameter decreased with increasing cooling rates: a) experiment 1, b) experiment 2, c) experiment 3, and d) experiment 4. This trend was also found for experiment series 2: e) experiment 5, f) experiment 6, and g) experiment 7.

remained nearly the same, whereas that of the lower PE was gradually reduced for increasing gradients. The choice of temperatures was analogous to those used from experiment 2 in the freeze-structuring of the alginate solutions (Figure 2a). The course of the cooling rate predicted by the a-factor (inset in Figure 8a) increased with increasing temperature gradients, as the overall system became colder with higher gradients. This could be confirmed experimentally for all concentrations and MWs. No significant difference was found between the different MWs (Figure 8b) or the different concentrations (Figure 8c).

Similar results were obtained in the case of PE temperatures 2. Here, the overall system became warmer with increasing temperature gradient, as the temperature of the lower PE remained constant, whereas that of the upper PE was gradually increased for higher gradients (temperatures analogous to alginate experiments, experiment 7, Figure 2d). Based on the a-factor, it was therefore expected that the cooling rate would decrease with increasing gradients (inset in Figure 8d), which was confirmed experimentally. However, again no clear difference in the magnitude of the cooling rates as a function of MW (Figure 8e) or concentration (Figure 8f) appeared.

3.2.3. SEM and Pore Size Distribution

An anisotropically aligned porous structure was found for all samples when observed by SEM (**Figure 9**). For the samples obtained in the experiments with PE temperatures 1, it was found that a too high viscosity prevented a controlled pore orientation (Figure 9a). Thus, for the samples prepared through structuring of a low-MW chitosan solution with a concentration of 2% (w/w), an

increasingly perpendicular orientation to the surface with an increasing temperature gradient was identified. This was consistent with the observations of the systematic investigations on alginate (Figure 4). However, when the concentration of the solution was doubled to 4% (w/w), no clear trend in the pore direction was evident. The pores, except for the smallest temperature gradient, were all oriented nearly perpendicular to the surface. Similar results were obtained for the high-MW 2% (w/w) samples. No clear dependence of pore orientation on the external temperature gradient was found, the pores were all oriented obliquely to the surface. In addition, it was observed for some samples that the pore orientation frequently changed inside the sample and domains with different orientations appeared.

A similar observation was made for samples freeze structured at PE temperatures 2 (Figure 9b). A tendency for pores oriented more perpendicular to the surface with increasing temperature gradient could only be confirmed for the low-MW 2% (w/w) samples. For scaffolds from the higher-concentrated low-MW 4% (w/w) solution, the pores were oriented perpendicular to the surface, especially for the higher gradients. 2% (w/w) samples from a high-MW solution exhibited pores oriented at an angle to the sample surface regardless of the external gradient. It was also noticeable here that an orientation change of the pores within the sample was found in some scaffolds.

Although a highly ordered, anisotropic pore structure could be observed for all samples (Figure 9a,b), a pore orientation controllable by the temperature gradient could thus only be ensured for both temperature ranges for the low-MW 2% (w/w) samples. This control was lost with higher viscosities. Another interesting observation was the occasional occurrence of different domains within the high-MW 2% (w/w) samples.
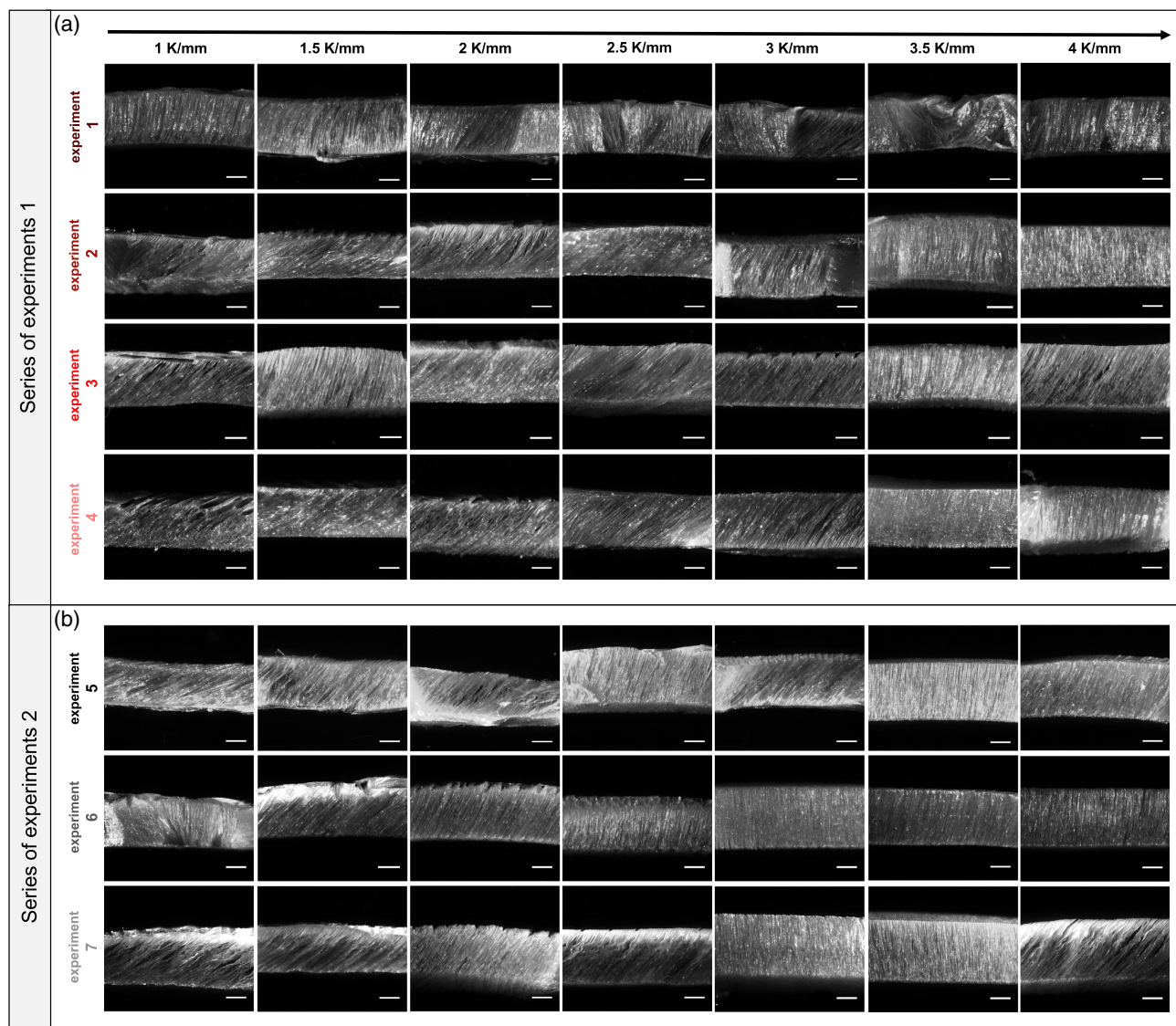
Figure 6. Stereomicroscopic cross-section images of ice-templated alginate samples. a) Examining larger areas of the samples of experiments series 1, no dependence of the pore orientation on the temperature gradient was found for experiment 1. Increasing the temperature gradient caused the pores to be increasingly oriented perpendicular to the surface in experiments 2–4. b) This trend was also found for the series of experiments 2. Scale bars in (a) and (b) are 1 mm.

Measurement of the pore diameters showed that pores of the low-MW 2% (w/w) samples tended to be the largest, followed by the 2% (w/w) high-MW scaffolds (Figure 9c). The samples prepared from the 4% (w/w) solutions tended to have the smallest pores. In general, the trend toward smaller pores with increasing external temperature gradient was also evident here for all sample types. Comparing the scaffolds prepared at the two different temperature ranges of the PEs, there was no significant difference between the pore sizes.

4. Discussion

In this study, the importance of the freezing parameter choice in directional freezing was highlighted, as this has a major impact on the process. It was shown that it is not sufficient to specify only the external temperature gradient used during the freezing process. Rather, factors such as the temperature of the overall system, the absolute temperatures of the cooling surfaces, and material properties such as the solution concentration, the MW, and consequently the viscosity must also be defined as these parameters have a significant influence on the process itself and the resulting scaffold morphology. Among other things, this study revealed that a too cold overall system during the freezing process, that is, temperatures of the lower cooling surface down to –60 °C combined with low temperatures of the upper cooling surface, led to a loss of control over pore orientation. This was also observed when using solutions with high viscosities above ≈5 Pas near the freezing point.
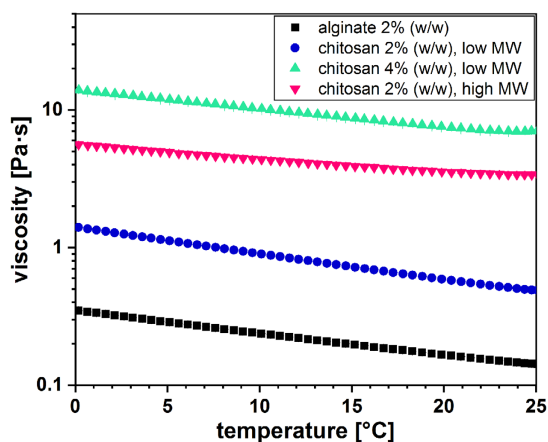
Figure 7. Viscosities of the polymer solutions used for directional freezing as a function of temperature. Viscosities of the alginate 2% (w/w), chitosan low-MW 2% (w/w), chitosan high-MW 2% (w/w), and chitosan low-MW 4% (w/w) solution are shown in black, blue, pink, and green, respectively.

It is known that the orientation of the aligned, anisotropic pores formed during directional freezing can be influenced by the choice of the external temperature gradient.[34] As the temperature gradient is determined only by the distance of the cooling surfaces as well as their temperature difference, the same

temperature gradient can be set by numerous different possible temperatures. However, to the best of our knowledge, a systematic investigation of the influence of the cooling surface temperatures on the resulting scaffold morphology is still lacking. To fill this gap, solutions of the biopolymers alginate and chitosan were directionally frozen in this study. For alginate, the influence of different temperature regimes on the resulting pore structure within the samples was investigated, whereas for the ice-templating of chitosan solutions, the focus was on the impact of different solution properties, such as concentration and MW and consequently the viscosity.

When comparing the results of the present study with those of other groups, it is important to note that there are a variety of options for freeze-structuring setups, complicating a direct comparison. For example, Yin et al. used a radial freeze-structuring apparatus to texture 3.5% (w/v) chitosan dissolved in 1.5% acetic acid for use as a ureteral stent.[43] The solution viscosity was not measured but given by the material supplier as 150–350 mPas for 1% (w/w) chitosan in 1% acetic acid at 20 °C. For structuring, the solution was placed in appropriate molds and frozen at –80 °C in a freezer. Neither the cooling rates nor the temperatures of the cooling surfaces were determined. However, the resulting morphology showed a multiplicity of domains,[43] which is consistent with our observations at low temperatures. The results presented in our study show that a more uniform pore structure can be achieved by selecting appropriate freezing parameters, such as the temperature of the overall system. For example, by choosing
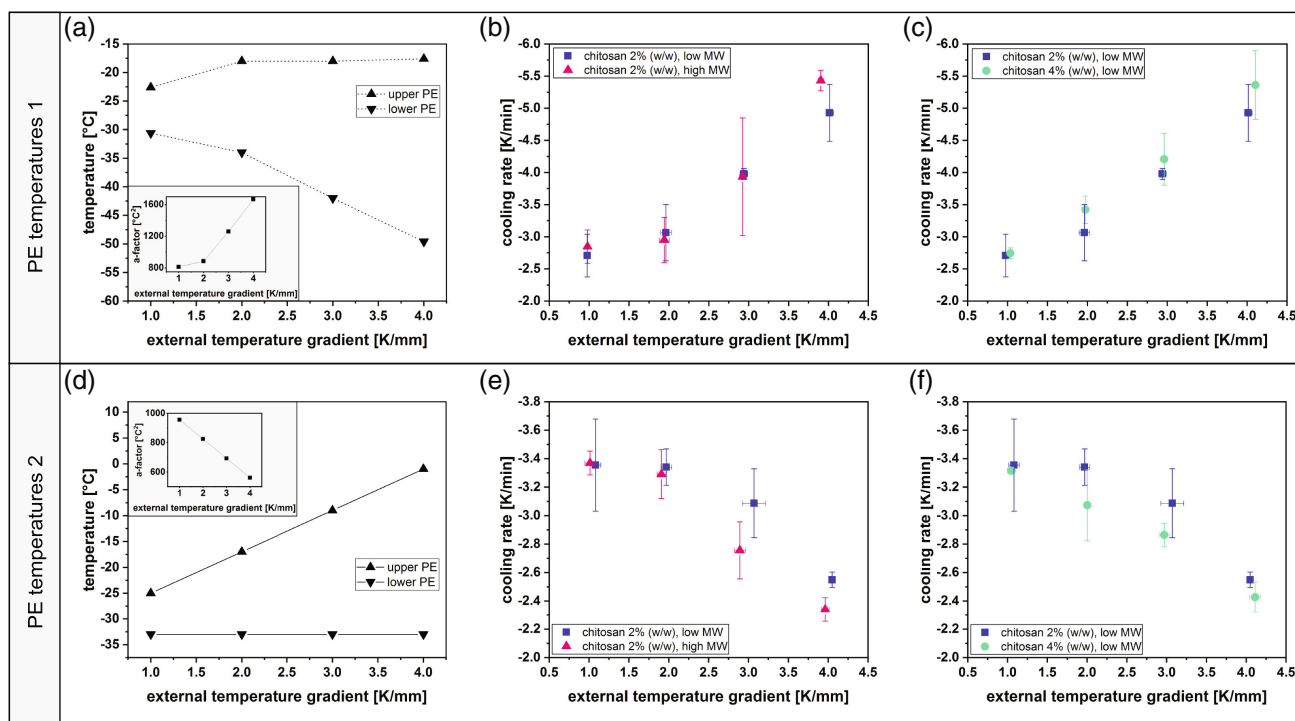

Figure 8. Cooling rate and a-factor of freeze-structured chitosan samples. a) For PE temperatures 1, the temperature of the upper PE remained largely constant, whereas that of the lower PE was decreased for increasing temperature gradients. According to the theoretical prediction by the a-factor (inset), the cooling rate increased with increasing temperature gradient. This was also observed experimentally for both b) different MWs (low MW [blue], high MW [pink]) and c) solution concentrations (2% (w/w) [blue], 4% (w/w) [green]). d) For PE temperatures 2, the temperature of the lower PE remained largely constant, whereas that of the upper PE was increased for higher gradients. The cooling rate predicted by the a-factor (inset) decreased with increasing gradient, which was also found experimentally for both e) different MWs and f) solution concentrations.
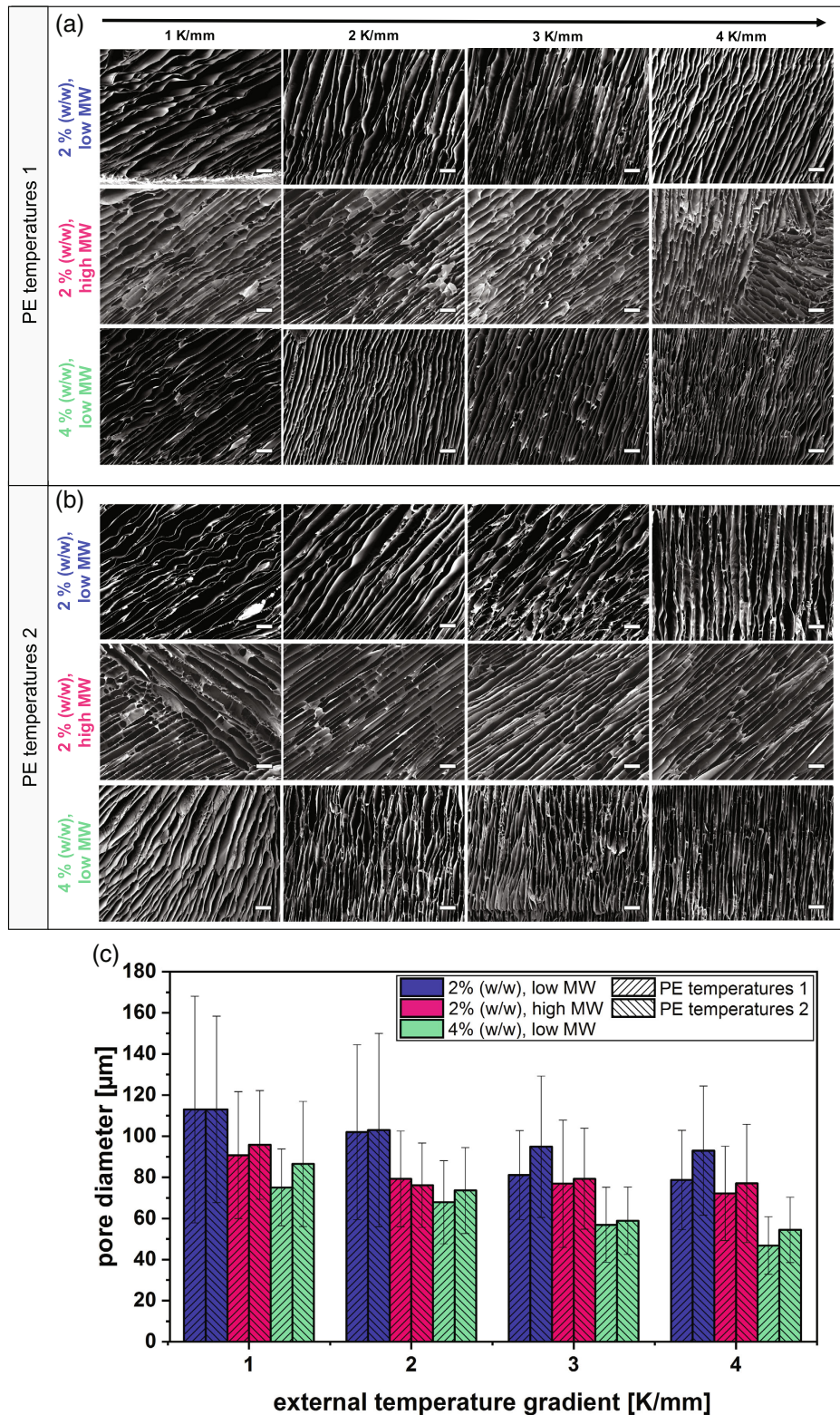
Figure 9. Pore orientation and diameter of directionally frozen chitosan samples. SEM cross-section images. a) At PE temperatures 1, an increasingly perpendicular orientation of the pores to the surface was observed with higher temperature gradients for the 2% (w/w), low-MW (blue) chitosan samples. For the 2% (w/w), high-MW (pink) and 4% (w/w), low-MW samples (green), no dependence of the pore orientation on the gradient was evident. b) A similar behavior was observed for the samples prepared at PE temperatures 2. c) With increasing temperature gradient, smaller pore diameters were observed. The largest pores were found for the 2% (w/w), low-MW chitosan samples, whereas freeze-structuring of 4% (w/w), low-MW solution led to the smallest pores. Scale bars in (a) and (b) are 200 μm.

not too low PE temperatures, the number of domains can be reduced (Figure 4 and Figure 6). In unidirectional freeze casting, ice crystals begin to nucleate in a disordered manner once the solution is injected on the cooled surface, which results in the observed different domains of varying orientations.[25,26] This effect is even more pronounced at lower surface temperatures, accelerating ice crystal nucleation and leading to a more heterogenous pore orientation as also observed in the present study. Solution viscosity also played a crucial role in the process, as texturing became more difficult, or pore alignment control was even lost at higher viscosities (Figure 9). This is consistent with a study from Florczyk et al., who investigated the influence of viscosities of chitosan-alginate solutions frozen in a freezer at −20 °C. It was found that a lower viscosity resulted in a more uniform pore structure.[44]

A study conducted by Francis et al. dealt with the directional freezing of a chitosan−alginate solution (1.5% [w/w]), using a PTFE mold placed on a cold finger being in contact with liquid nitrogen.[45] Here, the temperature of the cooled copper surface decreased with a cooling rate of $1\,°C\,min^{-1}$ until a temperature of −150 °C was reached. An external temperature gradient or the solution viscosity was not reported in the study. Regarding the MW, a range of 50–190 kDa and 270–325 kDa was given for chitosan and alginate, respectively.[45] Therefore, the MW of alginate was higher than that used in our study, whereas that of chitosan was similar to the low-MW chitosan. The freeze-dried scaffolds exhibited pore sizes of about 69 μm.[45] This was thus roughly in the size range of the pores observed in our study, which were found in alginate scaffolds frozen under an temperature gradient of $3\,K\,mm^{-1}$ (experiments 1 and 2) and $3\,K\,mm^{-1}$ or $4\,K\,mm^{-1}$ (experiments 5 and 6), respectively (Figure 4c,d). Here, the cooling rates lay between about −3.7 and $−5.6\,K\,min^{-1}$. In the present study, it was shown that the pore size can be adjusted by the temperature of the overall system as well as the solution properties. This allows the scaffold morphology to be specifically influenced and adapted to the intended application.

The influence of the applied cooling rates during directional freezing on the sample morphology, especially on the pore diameter, was investigated by Nematollahi et al. using freeze-structuring of silk−chitosan solutions.[46] Here, medium-MW chitosan, which was not specified further, was dissolved in 2% (w/v) acetic acid, mixed with silk solution in a ratio of 1:3 and directionally frozen using a PTFE mold on a copper cylinder connected to a liquid nitrogen bath. Freezing was conducted using the three different cooling rates 0.5, 1, and $2\,°C\,min^{-1}$. A decrease in pore diameter with increasing freezing rate was revealed.[46] This was also observed in the results presented in this study (Figure 4, Figure 5). A decreasing pore diameter with increasing freezing rates was also found by Christiansen et al.,[47] who used a freezing system similar to the device utilized in the present study.[47]

Pore orientation was assessed by Yin et al., who used a 3.5% chitosan solution in 1.5% (v/v) acetic acid inserted between two molds and then frozen at −80 °C to prepare tubular scaffolds with aligned porosity. Pores showed an orientation oblique to the freezing surfaces, as well as multiple domains with different pore orientations,[48] which is consistent with the findings in the present study, especially at low temperatures (Figure 4 and Figure 6). Again, the absolute temperatures of the freezing surfaces, the temperature gradient, the cooling rates, or the solution viscosity were not determined.

Considering all these comparisons, the importance of specifying the parameters used during directional solidification becomes apparent. The overall system, such as temperatures, temperature gradient, and freezing rates, but also solution properties such as viscosity must always be taken into account, as these factors can limit the process.

5. Conclusion

The aim of this study was to demonstrate that various parameters used in directional freezing have a significant influence on the resulting sample morphology and pore structure. Apart from the external temperature gradient, also the temperatures of the cooling surfaces, the cooling rate, as well as material properties such as the concentration, the MW (when using polymers), and the viscosity of the solution determine pore size and orientation after solidification. Here, inappropriate parameter settings may cause a loss of control over pore alignment during freezing, for example, when the temperature of the lower cooling surface goes below a limit of −60 °C or solution viscosity exceeds ≈5 Pas near the freezing point. Beyond these limitations, ice templating of alginate revealed that pore alignment could be controlled by the choice of the external temperature gradient, with a higher gradient leading to pores oriented increasingly perpendicular to the surface. The temperature of the overall system both influenced cooling rates and affected the pore diameters, leading to smaller pores at higher cooling rates. Although a custom-developed device was used for the systematic investigations presented in this study, the findings should also be applicable to other devices that offer the same frame conditions for unidirectional freeze-structuring.

Conflicts of Interest

The authors declare no conflict of interest.

Data Availability Statement

Research data are not shared.

Published online: August 29, 2021

[1] S. Deville, *Adv Eng Mater* **2008**, *10*, 155.

[2] S. Deville, *Materials* **2010**, *3*, 1913.

[3] S. Deville, *Scripta Mater* **2018**, *147*, 119.

[4] W. L. Li, K. Lu, J. Y. Walz, *Int Mater Rev* **2012**, *57*, 37.

[5] K. K. Qin, C. Parisi, F. M. Fernandes, *J Mater Chem B* **2021**, *9*, 889.

[6] K. L. Scotti, D. C. Dunand, *Prog Mater Sci* **2018**, *94*, 243.

[7] G. F. Shao, D. A. H. Hanaor, X. D. Shen, A. Gurlo, *Adv Mater* **2020**, *32*, 1907176.

[8] U. G. K. Wegst, M. Schecter, A. E. Donius, P. M. Hunger, *Philos T R Soc A* **2010**, *368*, 2099.

[9] R. P. Liu, T. T. Xu, C. A. Wang, *Ceram Int* **2016**, *42*, 2907.

[10] H. Joukhdar, A. Seifert, T. Jungst, J. Groll, M. S. Lord, J. Rnjak-Kovacina, *Adv Mater* **2021**, 2100091.

[11] Y. Bai, R. Liu, Y. M. Wang, H. H. Xiao, Y. Liu, G. H. Yuan, *Acs Appl Mater Inter* **2019**, *11*, 43294.

[12] Q. R. Wang, X. Y. Wang, F. Wan, K. N. Chen, Z. Q. Niu, J. Chen, *Small* **2018**, *14*, 1800280.

[13] P. K. Sahoo, N. Kumar, S. Thiyagarajan, D. Thakur, H. S. Panda, *Acs Sustain Chem Eng* **2018**, *6*, 7475.

[14] Y. Ni, J. Q. Qi, B. T. Zhou, L. Zhu, Y. J. Ren, D. Zhang, *J Mater Sci* **2021**, *56*, 7533.

[15] C. Stolze, T. Janoschka, S. Flauder, F. A. Muller, M. D. Hager, U. S. Schubert, *Acs Appl Mater Inter* **2016**, *8*, 23614.

[16] C. Huang, P. S. Grant, *J Mater Chem A* **2018**, *6*, 14689.

[17] P. Munier, V. Apostolopoulou-Kalkavoura, M. Persson, L. Bergstrom, *Cellulose* **2020**, *27*, 10825.

[18] V. Apostolopoulou-Kalkavoura, S. Q. Hu, N. Lavoine, M. Garg, M. Linares, P. Munier, I. Zozoulenko, J. Shiomi, L. Bergstrom, *Matter-Us* **2021**, *4*, 276.

[19] K. M. Pawelec, A. Husmann, S. M. Best, R. E. Cameron, *Mat Sci Eng C-Mater* **2014**, *37*, 141.

[20] W. L. Stoppel, D. J. Hu, I. J. Domian, D. L. Kaplan, L. D. Black, *Biomed Mater* **2015**, *10*, 034105.

[21] H. Rezaei, M. Shahrezaee, M. J. Monfared, F. Ghorbani, A. Zamanian, M. Sahebalzamani, *Biotechnol Appl Bioc* **2021**, *68*, 185.

[22] G. Nystrom, W. K. Fong, R. Mezzenga, *Biomacromolecules* **2017**, *18*, 2858.

[23] C. Rieu, C. Parisi, G. Mosser, B. Haye, T. Coradin, F. M. Fernandes, L. Trichet, *Acs Appl Mater Inter* **2019**, *11*, 14672.

[24] S. Christoph, J. Kwiatoszynski, T. Coradin, F. M. Fernandes, *Macromol Biosci* **2016**, *16*, 182.

[25] F. Bouville, E. Portuguez, Y. F. Chang, G. L. Messing, A. J. Stevenson, E. Maire, L. Courtois, S. Deville, *J Am Ceram Soc* **2014**, *97*, 1736.

[26] H. Bai, Y. Chen, B. Delattre, A. P. Tomsia, R. O. Ritchie, *Sci Adv* **2015**, *1*, e1500849.

[27] H. Bai, F. Walsh, B. Gludovatz, B. Delattre, C. L. Huang, Y. Chen, A. P. Tomsia, R. O. Ritchie, *Adv Mater* **2016**, *28*, 50.

[28] W. Z. Xu, Y. Xing, J. Liu, H. P. Wu, Y. Cuo, D. W. Li, D. Y. Guo, C. R. Li, A. P. Liu, H. Bai, *Acs Nano* **2019**, *13*, 7930.

[29] I. Nelson, T. A. Ogden, S. Al Khateeb, J. Graser, T. D. Sparks, J. J. Abbott, S. E. Naleway, *Adv Eng Mater* **2019**, *21*, 1801092.

[30] Y. F. Tang, S. Qiu, Q. Miao, C. Wu, *J Eur Ceram Soc* **2016**, *36*, 1233.

[31] T. A. Ogden, M. Prisbrey, I. Nelson, B. Raeymaekers, S. E. Naleway, *Mater Design* **2019**, *164*, 107561.

[32] M. C. Gutierrez, M. L. Ferrer, F. del Monte, *Chem Mater* **2008**, *20*, 634.

[33] H. F. Zhang, J. Long, A. I. Cooper, *J Am Chem Soc* **2005**, *127*, 13482.

[34] K. Stuckensen, A. Schwab, M. Knauer, E. Muinos-Lopez, F. Ehlicke, J. Reboredo, F. Granero-Molto, U. Gbureck, F. Prosper, H. Walles, J. Groll, *Adv Mater* **2018**, *30*, 1706754.

[35] V. Karageorgiou, D. Kaplan, *Biomaterials* **2005**, *26*, 5474.

[36] S. F. Hulbert, F. A. Young, R. S. Mathews, K. J. C. D. Talbert, F. H. Stelling, *J Biomed Mater Res* **1970**, *4*, 433.

[37] C. M. Murphy, M. G. Haugh, F. J. O'Brien, *Biomaterials* **2010**, *31*, 461.

[38] J. J. Campbell, A. Husmann, R. D. Hume, C. J. Watson, R. E. Cameron, *Biomaterials* **2017**, *114*, 34.

[39] S. Muehleder, A. Ovsianikov, J. Zipperle, H. Redl, W. Holnthoner, *Front Bioeng Biotechnol* **2014**, *2*, 52.

[40] K. Stuckensen, U. Gbureck, J. Groll, EP2788171A2, **2021**.

[41] T. Waschkies, R. Oberacker, M. J. Hoffmann, *J Am Ceram Soc* **2009**, *92*, S79.

[42] T. Waschkies, R. Oberacker, M. J. Hoffmann, *Acta Mater* **2011**, *59*, 5135.

[43] K. Y. Yin, P. Divakar, U. G. K. Wegst, *Acta Biomater* **2019**, *84*, 231.

[44] S. J. Florczyk, D. J. Kim, D. L. Wood, M. Q. Zhang, *J Biomed Mater Res A* **2011**, *98*, 614.

[45] N. L. Francis, P. M. Hunger, A. E. Donius, B. W. Riblett, A. Zavaliangos, U. G. K. Wegst, M. A. Wheatley, *J Biomed Mater Res A* **2013**, *101*, 3493.

[46] Z. Nematollahi, M. Tafazzoli-Shadpour, A. Zamanian, A. Seyedsalehi, S. Mohammad-Behgam, F. Ghorbani, F. Mirahmadi, *Iran Biomed J* **2017**, *21*, 228.

[47] C. D. Christiansen, K. K. Nielsen, R. Bjork, *Rev Sci Instrum* **2020**, *91*, 033904.

[48] K. Yin, P. Divakar, J. Hong, K. L. Moodie, J. M. Rosen, C. A. Sundback, M. K. Matthew, U. G. K. Wegst, *MRS Adv* **2018**, *3*, 1677.